Research Article | Vol. 27, No. 5 | 4 Mar 2019 | OPTICS EXPRESS 7072
Optics EXPRESS

Modulation format identification assisted by sparse-fast-Fourier-transform for hitless flexible coherent transceivers

JIANING LU,[1,*] ZHONGWEI TAN,[1] ALAN PAK TAO LAU,[2] SONGNIAN FU,[3] MING TANG,[3] AND CHAO LU[1]

[1]*Photonics Research Centre, Department of Electronic and Information Engineering, The Hong Kong Polytechnic University, Hung Hom, Kowloon, Hong Kong*
[2]*Photonics Research Centre, Department of Electrical Engineering, The Hong Kong Polytechnic University, Hung Hom, Kowloon, Hong Kong*
[3]*National Engineering Laboratory of Next Generation Internet Access Networks, School of Optical and Electronic Information, Huazhong University of Science and Technology, Wuhan 430074, China*
[*]*jianing.lu@connect.polyu.hk*

Abstract: For hitless flexible coherent transceivers based next-generation agile optical network, efficient modulation format identification (MFI) is an essential element in digital signal processing (DSP) flow at the receiver-side (Rx). In this paper, we propose a blind and fast MFI scheme with high identification accuracy at low optical signal-to-noise ratio (OSNR) regime. This is achieved by first raising the signal to the 4th power and calculate the peak-to-average power ratio (PAPR) of the corresponding spectra to distinguish 32 quadrature amplitude modulation (QAM) from quadrature phase shift keying (QPSK), 16 and 64QAM signals. Then, followed by iterative partition schemes to remove signals with phase $\pm\frac{\pi}{4},\pm\frac{3\pi}{4}$ (or QPSK-like phases) based on the signal amplitudes, the PAPR of the remaining signals is calculated to distinguish the other three formats. Additionally, by frequency offset (FO) pre-compensation, the spectrum can be obtained using sparse-fast-Fourier-transform (S-FFT), which greatly reduces the total complexity. The MFI performance is numerically and experimentally investigated by 28 Gbaud dual-polarization (DP) coherent optical back-to-back (B2B) and up to 1500 km standard single mode fiber (SSMF) transmission system using QPSK, 16QAM, 32QAM, and 64QAM. Results show that high identification accuracy can be achieved, even when OSNR is lower than that required for the 20% forward error correction (FEC) threshold of BER=2×10^{-2} for each format. Furthermore, fast format switching between 64QAM-32QAM and 32QAM-16QAM are demonstrated experimentally for B2B scenario and 900 km SSMF with the proposed MFI technique, respectively.

1. Introduction

To accommodate increasingly heterogeneous traffic and better adapt transmissions to real-time link conditions such as environmental change, aging etc, current fixed optical networks are expected to evolve to future flexible and adaptive optical networks [1–3]. For flexible optical networks, hitless flexible coherent transceiver is proposed to realize adaptive rate transmission through modulation format switching according to current link margin and traffic requirements without the transmission interruption [4–6]. Hitless flexible coherent transceiver is expected to improve the total capacity and reduce energy consumption. In this connection, efficient modulation format identification (MFI) is critical to reconfigure the digital signal processing (DSP) flow at the receiver side (Rx) [6–8].

Generally, the existing proposed MFI schemes can be divided into three main categories. The first kind employs time-domain features of different standard quadrature amplitude

#357083 https://doi.org/10.1364/OE.27.007072
Journal © 2019 Received 9 Jan 2019; revised 15 Feb 2019; accepted 15 Feb 2019; published 25 Feb 2019

Optics EXPRESS

modulation (QAM) formats as the identification criteria [7–15]. The features include distributions or histograms of amplitude and phase etc. For dual-polarization (DP) signals, the Stokes-space-based method, which firstly maps the signal to 3-D Stokes-space according to its distribution of amplitude and phase and identify the format by the total number of clusters [9–11]. Histogram of amplitude has also been used [12,13] but it requires large number of symbols to achieve high accuracy, thus prohibiting fast format switching. Meanwhile, for high-order format under low optical signal-to-noise ratio (OSNR), MFI performance degrades severely. For the case of Stoke space-based MFI, the cluster number would rapidly increase to 244/996 for 32/64QAM, which causes huge difficulty and high complexity for MFI in presence of additive white Gaussian noise (AWGN) at low OSNRs. This kind of MFI method is sometimes combined with machine learning methods such as support vector machine and neural networks [12]. However, machine learning methods will be problematic in such MFI. Firstly, huge amount of training samples is required to train a network specific to one particular link. Moreover, the trained network may not be suitable anymore when the link conditions such as distance or other parameter changes. To guarantee high MFI accuracy, machine learning models should be retrained whenever the link is changed, which is resource consuming and not practical. The second type of MFI is data-aided (DA) scheme, which is realized with training symbols [7] or extra sub-carrier pilots [8]. It is more robust than the first type and is capable of tracking fast format switching. However, the spectral efficiency (SE) is sacrificed. Recently, signal spectrum-based MFI is proposed [14,15] and it works well at low OSNR conditions due to the robustness of the spectrum to noise. In [14], after the nonlinear power transformation of different orders and fast-Fourier-transform (FFT), MFI is performed through peak searching in the spectra. Due to multiple n^{th} power operation of signals and FFT, the complexity is high and high order formats beyond 16QAM are still hard to be identified. In [15], the format information is coded to frequency offset (FO) distribution of the signal at the transmitter-side (Tx). However, chromatic dispersion (CD) estimation would be affected because of the fast-changing FO [15]. Considering MFI for hitless flexible coherent transceiver, a blind, fast, and low-complexity MFI scheme with high accuracy even for high-order formats is worthy of further study.

In this paper, we propose a blind and efficient MFI scheme which supports quadrature phase shift keying (QPSK), 16QAM, 32QAM, and 64QAM formats and operates in the frequency domain. Different constellation partition schemes are applied to the received signals followed by 4th power operation. The peak-to-average power ratio (PAPR) of the spectra is calculated to determine the occurrence of a peak, which is taken as the criteria to distinguish different formats. The process is repeated in a sequential manner to identify all the formats. After the FO pre-compensation, the spectra can be calculated using the sparse-FFT (S-FFT) [16,17], leading to substantial reduction of the total complexity. We carry out both simulations and experiments to investigate the performance of the proposed MFI in 28 Gbaud dual-polarization (DP) back-to-back (B2B) and up to 1500 km standard single mode fiber (SSMF) transmission system. High identification accuracy for QPSK, 16/32/64QAM are obtained even when the OSNR is lower than the value required for the 20% forward error correction (FEC) of BER=2×10^{-2} for each format. The impact of the sparsity in S-FFT is also studied. The proposed MFI shows better performance than the existing MFIs based on Stokes-space [9] and power distribution [13]. A hitless flexible coherent transceiver with fast format switching between 64QAM-32QAM and 32QAM-16QAM for B2B and over 900 km SSMF transmission are demonstrated, respectively. Assisted by the proposed MFI, the length of switching-block is shortened to 1024 symbols. Finally, the analysis of computational complexity to realize the MFI is presented.

Optics EXPRESS

2. Operating principle

2.1 Modulation format identification by spectra peak search

In the Rx DSP flow of hitless flexible coherent transceiver, the proposed MFI is implemented after format-transparent constant modulus algorithm (CMA) based equalization. Assuming the ideal clock recovery, and equalization, the received signal $r(n)$ can be expressed as [18]

$$r(n) = m(n)\exp(j(\Delta\omega nT + \theta(n))) + v(n), n = 0,1,2,\ldots \quad (1)$$

where $m(n)$ represents the n^{th} modulated data symbol, T is the symbol period, $\Delta\omega = 2\pi\Delta f$ is the angular FO where Δf is the FO. $\theta(n)$ is the laser phase noise, which is induced by linewidth of the transmitter/local oscillator (LO) lasers and $v(n)$ is AWGN. In order to estimate and compensate the FO, FFT based FO estimation (FFT-FOE) method is generally employed. For square QAM, the estimated frequency value $\Delta\hat{f}$ based on FFT-FOE is given by

$$\Delta\hat{f} = \frac{1}{4}\cdot\frac{1}{TN}\arg\max_{k,|k|\le N/2}\left|R_4(f)\right| = \frac{1}{4}\cdot\frac{1}{TN}\arg\max_{k,|k|\le N/2}\left|\sum_{n=0}^{N-1} r^4(n)e^{-j\frac{2\pi nk}{N}}\right| \quad (2)$$

where $R_4(f)$ is the spectrum of $r^4(n)$. N is the length of the signal. Equation (2) leads to a process to search the intensity peak in the periodogram of $r^4(n)$, which can be implemented by FFT [19]. For QPSK signal, as shown in Fig. 1(a), the phases are $[-3\pi/4, -\pi/4, +\pi/4, +3\pi/4]$. By the 4th power transformation, the phase of $m(n)$ can be removed and the FO value can be obtained by locating the peak in the spectrum of $r^4(n)$. As for 16QAM or 64QAM signal, there are 2 and 4 rings of points whose phases resemble the QPSK constellation (red points in Figs. 1(b) and 1(d)) and can be removed by the 4th power transformation. We denote these points as QPSK-like points for the rest of the paper. Among these points, four points at each corner are of the maximum amplitude. As shown in Eq. (2), these points make the most contribution to the peak intensity. On the other hand, the distribution of residual points is symmetrically with respect to the diagonal line with slope equal to + 1 or −1, eliminating the disturbance to the intensity peak. Therefore, FFT-FOE is still effective even though $m^4(n)$ is not constant [19].

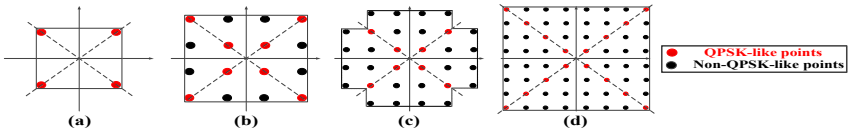

Fig. 1. Constellations of (a) QPSK, (b) 16QAM, (c) 32QAM, (d) 64QAM.

However, FFT-FOE is not suitable for 32QAM with a limited FFT size due to the non-rectangular distribution of constellation points. As shown in Fig. 1(c), without the important contributions from QPSK-like points of maximum amplitude at four corners, the peak in spectrum suffers from severe distortions. Figures 2(a)-2(d) show the 4th power spectra of 28 Gbaud QPSK, 16QAM, 32QAM, and 64QAM with FFT size of 512, respectively. It is observed that there are lots of interference peaks in the 4th power spectrum of 32QAM, while the peak is obvious for the other three formats. Therefore, we can use this feature to distinguish 32QAM among these four formats. To realize an effective MFI scheme for a wide OSNR range in flexible optical networks, a proper criterion should be used to decide whether

Optics EXPRESS

there is a peak or not in the spectrum. We propose to calculate a slightly modified PAPR of $R_4(f)$ defined as

$$PAPR=\frac{\max\limits_k |R_4(f)|}{\left(\sum\limits_{k=0}^{N-1}|R_4(f)|-\max\limits_k |R_4(f)|\right)\Big/(N-1)} \tag{3}$$

Here, we remove the peak value for the denominator to avoid error induced by different FFT-size. Then the calculated PAPR is more appropriate for the decision in MFI. Figure 3(a) shows the PAPR for four formats within the OSNR from 5 to 30 dB. The PAPR of 32QAM is lower than that of other formats when the OSNR is larger than 10 dB, indicating that the peak searching by PAPR calculation can be used as the identification criteria. The PAPR threshold is set to decide whether there is a peak or not. The optimization of threshold is presented in Section 3.1.

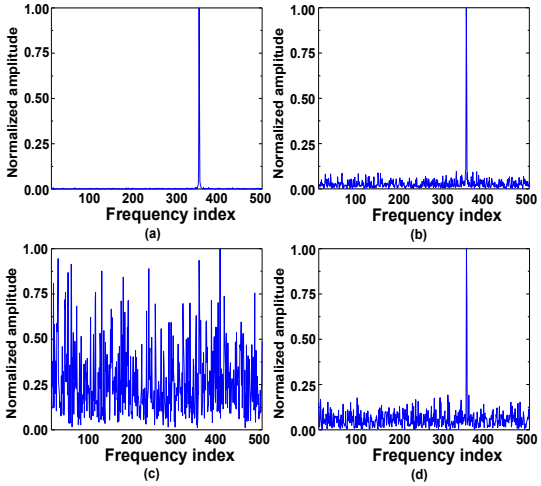

Fig. 2. 4th power spectra of (a) QPSK, (b) 16QAM (c) 32QAM and (d) 64QAM. OSNR is 19.3 dB with the 0.1 nm resolution. The symbol rate is 28 Gbuad. The FO is 1.4 GHz.

Next, we need to distinguish between QPSK, 16QAM, and 64QAM, which all have peak in the 4th power spectrum. Inspired by the analysis above, we proposed to use two constellation partition schemes after CMA equalization and the power normalization. The partition scheme I is used to distinguish 64QAM from QPSK and 16QAM while the partition scheme II distinguishes 16QAM from QPSK. For the 64QAM constellation, there are 9 rings with corresponding amplitude of 0.2180, 0.4874, 0.6539, 0.7859, 0.8987, 1.0899, 1.1738, 1.3259 and 1.5258 after the power normalization. Among these rings, the 1st, 3rd, 6th, and 9th ring consist of QPSK-like points. Considering that QPSK-like points have important contributions to the FO peak, partition scheme I selects these points according to their amplitudes and set them to zero in the calculation of the spectrum. For this step, the FFT size is decreased to 256 to enhance the impact of lost QPSK-like points. The PAPR of the corresponding spectra as a function of OSNR are shown in Fig. 3(b). With the help of the partition scheme I, the PAPR of 64QAM spectrum decreases rapidly. The insets of Fig. 3(b) show the corresponding 4th power spectra. The OSNR is 21.9 dB to reach the BER of 2×10^{-2} for 64QAM. It is observed that, the spectrum of 64QAM suffers from severe interference. On the other hand, the impact of partition scheme I to spectra of QPSK and 16QAM is minimal.

After the identification for 32QAM and 64QAM, we further employ the partition scheme II to distinguish 16QAM from QPSK. Similar as the partition scheme I, the QPSK-like points,

Optics EXPRESS

which are located at the 1st ring and the 3rd ring in 16QAM after CMA, are selected and set them to zero. Figure 3(c) shows the PAPR curves of corresponding spectrum for QPSK and 16QAM with the partition scheme II. The insets of Fig. 3(c) show the 4th power spectra of QPSK and 16QAM, when the OSNR is 16.2 dB to reach the BER of 2×10^{-2} for 16QAM and the FFT size is 512. Therefore, QPSK and 16QAM can be distinguished.

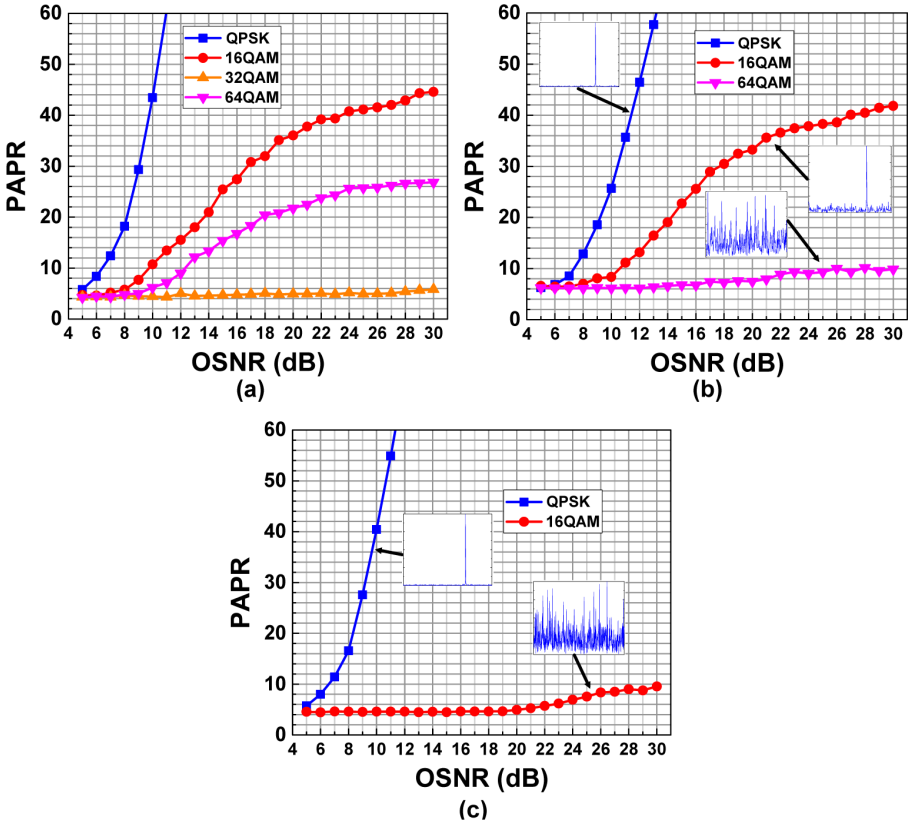

Fig. 3. (a) PAPR of the 4th power spectra for QPSK, 16, 32 and 64QAM. The FFT size is 512. (b) PAPR of 4th power spectra for QPSK, 16 and 64QAM, with the partition scheme I. The inserted figures are the 4th power spectra with OSNR of 21.9 dB. The FFT size is 256. (c) PAPR of the 4th power spectra for QPSK and 16QAM, with the partition scheme II. The inserted figures are the 4th power spectra with OSNR of 16.2 dB. The FFT size is 512.

Overall, by calculating the PAPR of the 4th power spectrum with/without the partition scheme I and the partition scheme II, we can perform MFI between QPSK, 16QAM, 32QAM, and 64QAM. The decision flow chart of proposed MFI is shown in Fig. 4. As it shows, 32 QAM signal can be firstly identified at step 1 without partition schemes, while the MFI for 64QAM signal can be conducted before the partition scheme II. If a signal is 16QAM or QPSK signal, it can be recognized at the last step. To achieve good MFI accuracy over a wide OSNR range, the PAPR threshold of each step (Th1, Th2, Th3) should be carefully optimized. Here, signals from both polarizations can be used to calculate the PAPR, enhancing the robustness of the MFI. In this paper, we conduct MFI for a block length of 1024 symbols from both polarizations. Under the condition of no partition and partition scheme II, totally four spectrums with a length of 512 are summed up for the PAPR calculation, while for the partition scheme I, eight spectrums with a length of 256 are used.

Optics EXPRESS

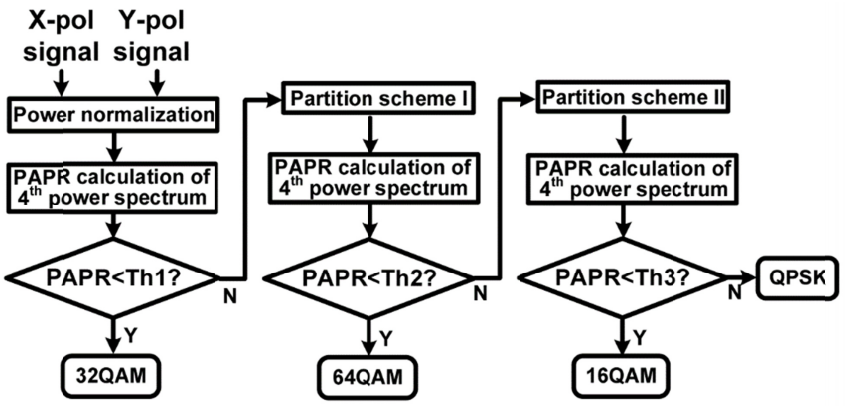

Fig. 4. Decision flow chart of the proposed MFI.

2.2 Low complexity spectrum and PAPR calculation assisted by S-FFT

Sparse-FFT aims to estimate the k largest (in magnitude) coefficients of the FFT of a vector x with length of n. Consequently, the high complexity of FFT can be reduced, and a coarse spectrum can be obtained [16]. Considering that the FO spectrum has only one peak, we employ a simple type S-FFT to reduce the total complexity of MFI [17]. Firstly, we introduce a basic property of Fourier transform, which is well-known in computing science: Aliasing a signal in the time domain is equivalent to subsampling it in the frequency domain, and vice versa. Figure 5 illustrates this property for the signal length of 8.

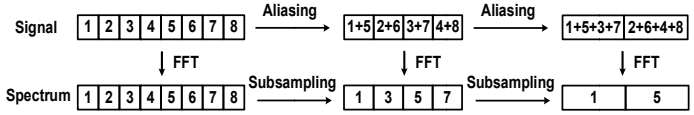

Fig. 5. Schematic of time domain aliasing and frequency domain subsampling.

Taking Fig. 5 as an example, for a signal length of $2n\times 2$ (n is an integer), the frequency components at index of odd numbers are retained after once signal aliasing, while the even components are lost. For the retained components, their indexes in the subsampled spectrum is $(i_p + 1)/2$, where i_p is the previous index in the spectrum before subsampling.

Based on above analysis, we can concluded that for the signal length of 2^n, the frequency component whose index is $2^{n-1}+1$ will never lose no matter how many times aliasing and subsampling are performed (e.g. the 5th frequency component in Fig. 5). On the other hand, for a direct current (DC) or no-FO signal with a length of 2^n, the only peak in the spectrum is right located at $2^{n-1}+1$. By taking advantage of this characteristic, we can reduce the complexity of spectrum calculation. For the proposed MFI, three times calculation of spectrum are required for the with/without the partition scheme I and II. For the first step, it is as same as the FFT-FOE and we can perform the FO compensation (FOC) to the 4th power signal using the estimated FO value. Then, the FO peak of the spectrum with the partition scheme I and II is located at $2^{n-1}+1$, and will always exist in the subsampled spectrum. In practice, the phase noise induced by lasers can also change the phase or even the FO of signals. Fortunately, when we use FFT-FOE to estimate the FO of the signal, the impact of phase noise has been included in the estimated FO value. Therefore, our proposed MFI scheme is insensitive to the effect of laser linewidth. Figure 6(a) shows the 4th power spectrum of QPSK without partition and Fig. 6(b) shows the 4th power spectrum of the same signal as in Fig. 6(a) with the FOC and partition scheme II. Figures 6(c)-6(f) depict spectra obtained by S-FFT with the subsampling rate p of 4, 16, 64, and 256, respectively, and the

Optics EXPRESS

peak is located at 65, 17, 5, 2, respectively, which accords with the iteration relationship of (index$_p$ + 1)/2. Therefore, full-point FFT can be avoided in the last two steps with the partition scheme I and II. S-FFT can be used to calculate the spectrum with shorter FFT-size after the signal aliasing. With this kind of S-FFT, the DC-frequency component and non-DC frequency components can be simultaneously obtained to calculate PAPR efficiently. The subsampling rate p of S-FFT should be optimized taken both the complexity and MFI performance into account.

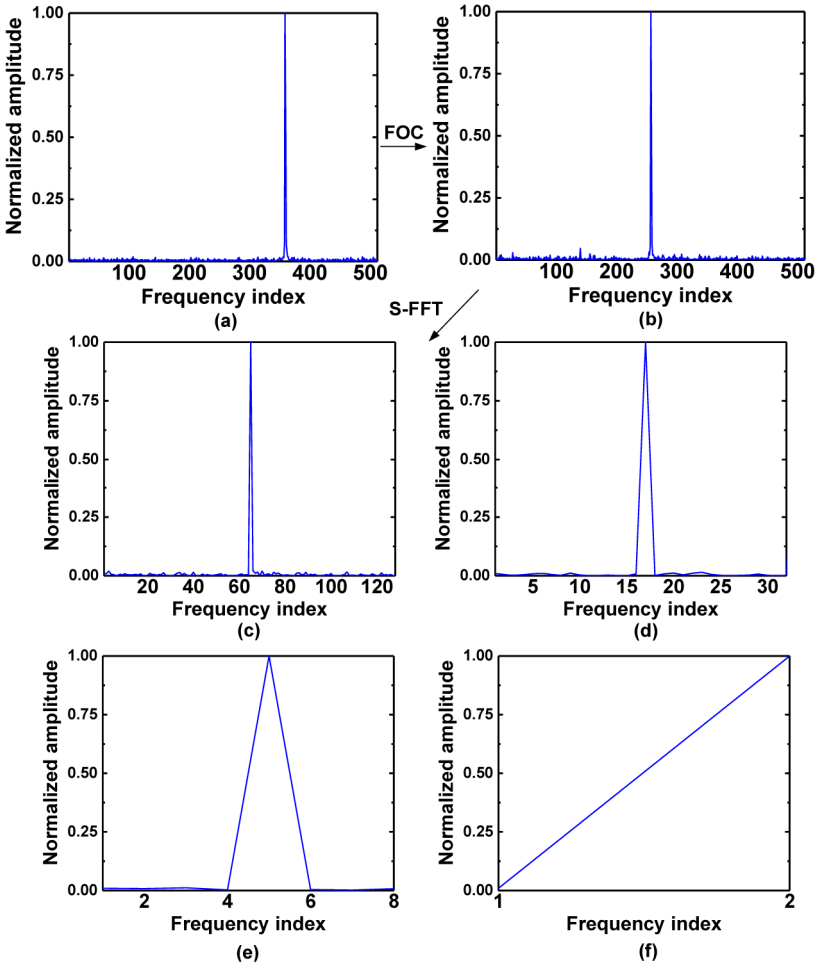

Fig. 6. (a) Spectra for 4th power of QPSK signals without partition, (b) Spectra of the signal in (a) with FO compensation and partition scheme II. Spectra obtained by S-FFT with the subsampling rate p of (c) 4, (d) 16, (e) 64, (f) 256. FFT size is 512. OSNR is 16.2 dB

3. Simulation results and optimization

3.1 Impact of threshold setting

We study the impact of threshold setting to the MFI accuracy. The combined laser linewidth is set to 200 kHz. For the first step, threshold (Th1) should be optimized to maximize the correct identification probability of 32QAM and minimize the false alarm probability of other three formats. Probability for one OSNR value is obtained by 2000 independent simulations. Figures 7(a)-7(d) shows the correct identification probability of DP-32QAM and the false alarm probability of DP-QPSK/16QAM/64QAM, respectively, with PAPR threshold setting

Optics EXPRESS

from 7 to 12. The theoretical OSNR limit to reach BER=2×10^{-2} is also plotted as a reference. As shown in Fig. 7(a), if the PAPR threshold is lower than 9, the correct identification probability degrades at high OSNRs because the PAPR of 4th power spectrum increases as shown in Fig. 3. On the other hand, we can see from Figs. 7(b)-7(d) that the false alarm events are more likely to happen when the PAPR threshold is set higher for DP-QPSK/16QAM/64QAM. Taking this trade-off into account, we choose 9 as the Th1 for the MFI without the use of partition scheme.

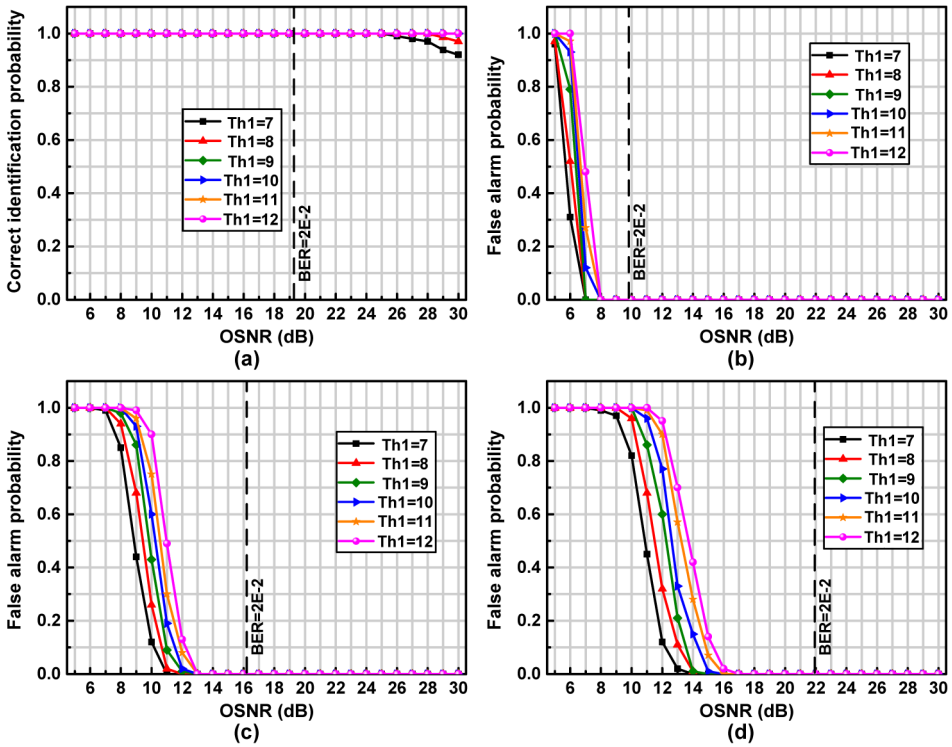

Fig. 7. (a) Correct identification probability of DP-32QAM, (b)-(d) the false alarm probability of DP-QPSK, DP-16QAM, and DP-64QAM, respectively, without partition scheme.

Optics EXPRESS

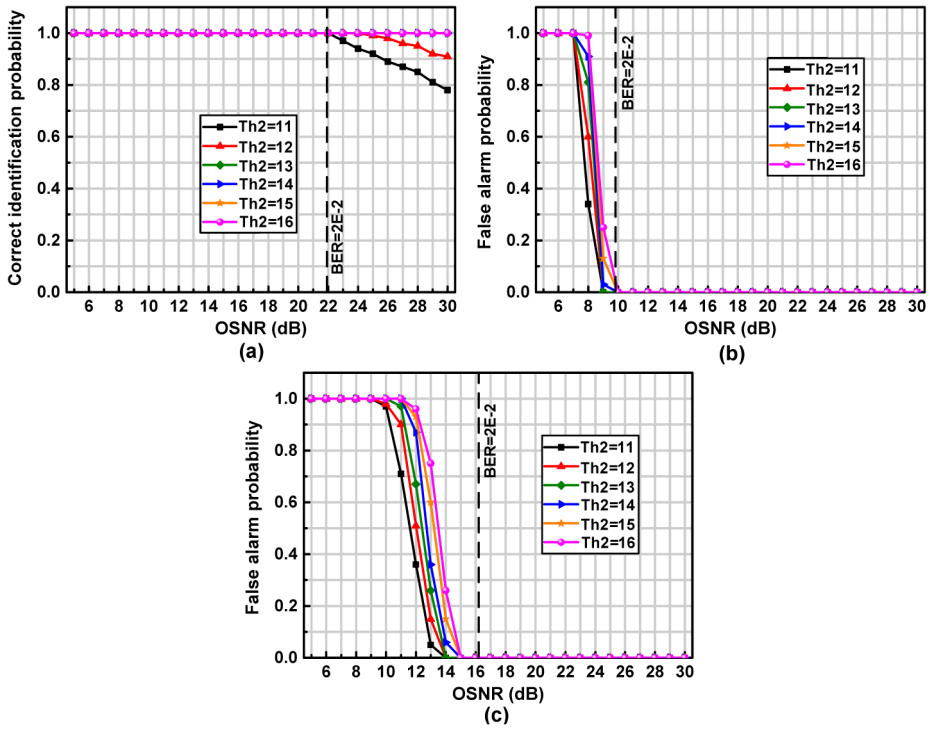

Fig. 8. (a) Correct identification probability of DP-64QAM, (b)-(c) the false alarm probability of DP-QPSK, and DP-16QAM, respectively, with the partition scheme I.

Then, for the second step with the partition scheme I, threshold (Th2) should be optimized according to the correct identification probability of DP-64QAM and the false alarm probability of DP-QPSK/16QAM, as plotted in Fig. 8(a)-8(c), respectively. The principle of optimization is the same as that in the first step. The optimal choice of the Th2 is 13. Finally, we optimize the PAPR threshold for the third (Th3) step using the partition scheme II. Figures 9(a)-9(b) show the correct identification probability of DP-16QAM and the false alarm probability of DP-QPSK, respectively. Similarly, we choose 14 as the threshold for the third step. Overall, the PAPR thresholds Th1, Th2, and Th3 for 3 steps are set to 9, 13, and 14, respectively.

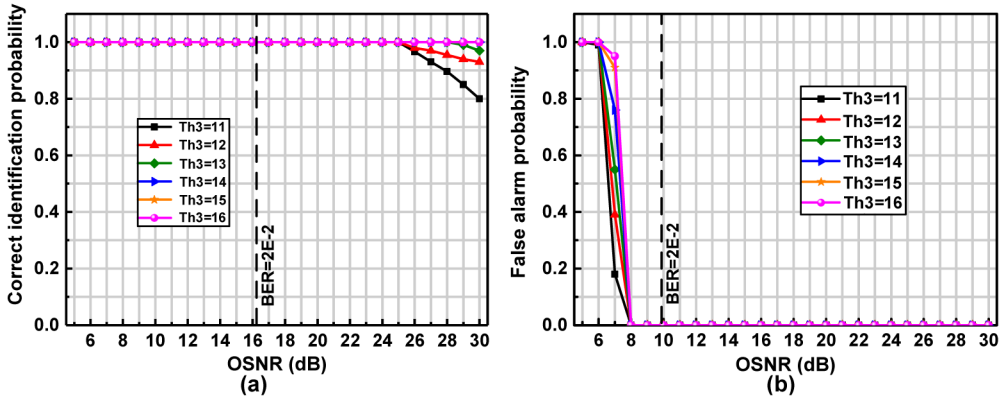

Fig. 9. (a) Correct identification probability of DP-16QAM, (b) the false alarm probability of DP-QPSK, with the partition scheme II.

Optics EXPRESS

3.2 Impact of subsampling rate

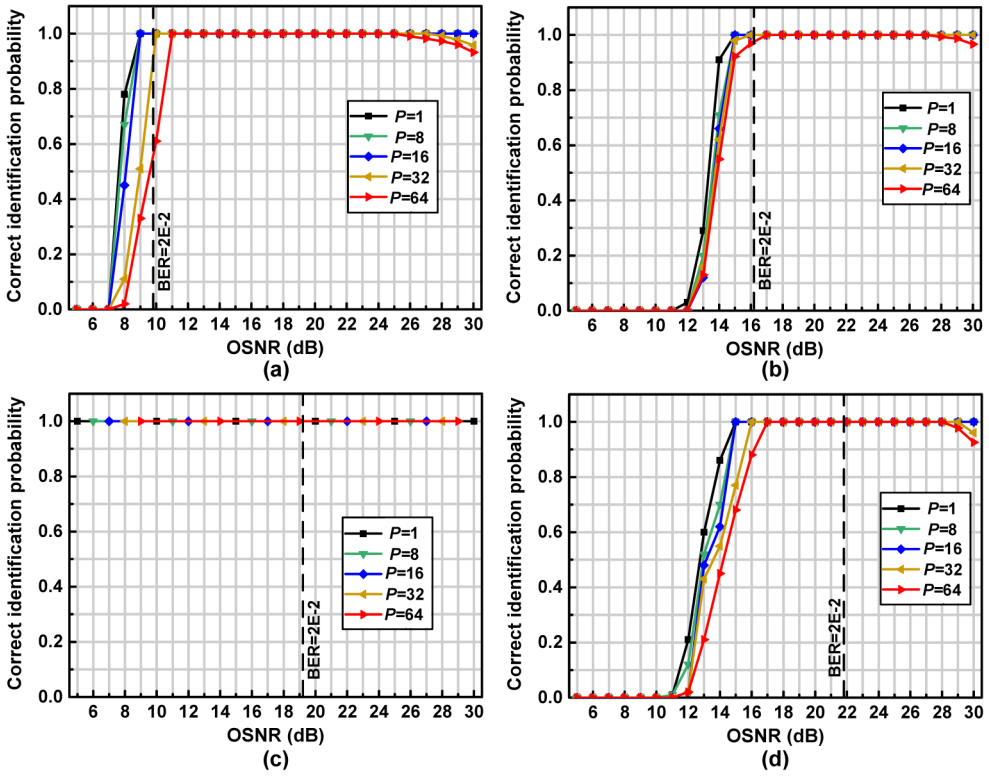

Fig. 10. Correct identification probability of (a) DP-QPSK, (b) DP-16QAM, (c) DP- 32QAM, and (d) DP-64QAM, with different subsampling rate p.

As analyzed above, the spectra in the step 2 and step 3 can be calculated using S-FFT. The subsampling rate p should be optimized to reduce the complexity as much as possible, while maintaining the MFI accuracy. If p is high, the correction identification probability will be affected because after S-FFT, we calculate the PAPR in a smaller-size spectrum, resulting in more variance of $\left(\sum_{k=0}^{N-1}|R_4(f)|-\max_k|R_4(f)|\right)\Big/(N-1)$ in Eq. (3), although the peak value is unaffected. Here, with the optimal PAPR thresholds setting, Figs. 10(a)-10(d) show the correct identification probability versus OSNR for DP-QPSK/16QAM/32QAM/64QAM with different subsampling rates. The proposed MFI can provide 100% accuracy for four formats at the OSNR lower than that required for the corresponding theoretical 20% FEC limit of BER=2×10^{-2}, with the p of 1 (full-point FFT). The accuracy of DP-32QAM is not affected by the subsampling rate because it is identified at the first step where full-point FFT is necessary. When the p is 16 or lower, there is no obvious performance degradation for other three formats. Therefore, the subsampling rate p of 16 is chosen to realize S-FFT for low-complexity MFI.

Optics EXPRESS

4. Experimental results

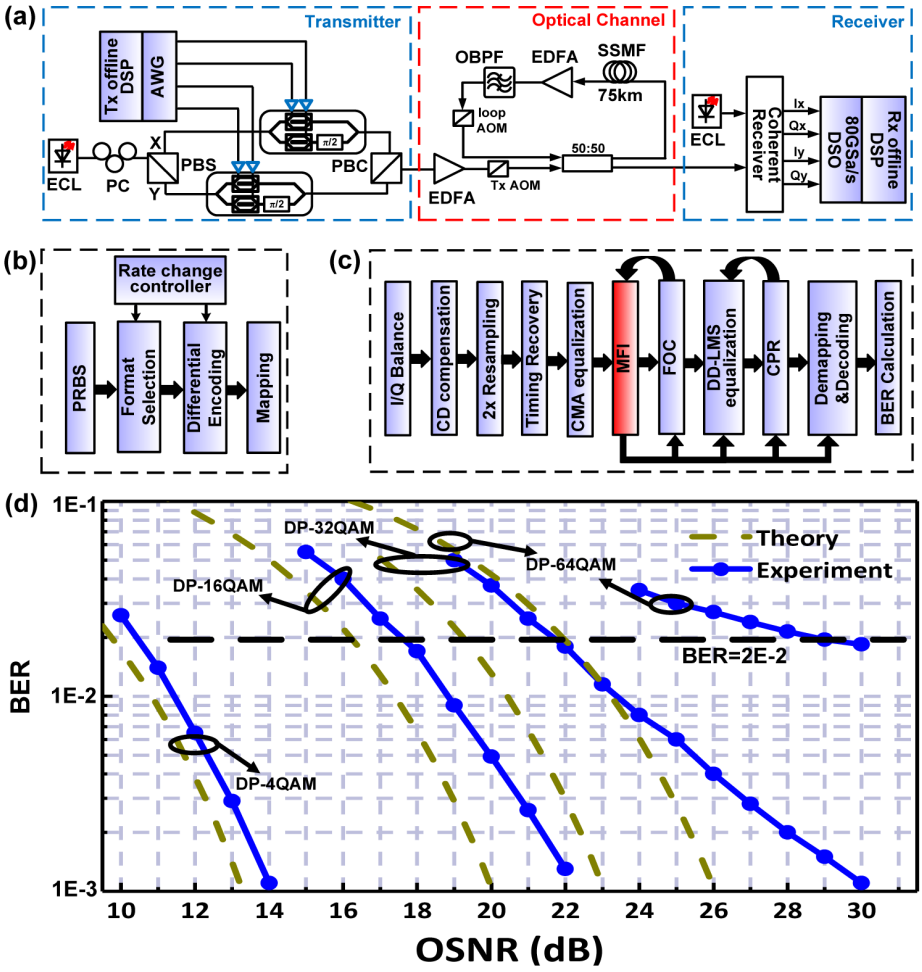

Fig. 11. (a) Experimental setup of hitless coherent transceiver, the offline DSP at the (b) Tx and (c) Rx. (d) measured B2B performance. (AOM: acousto-optic modulator, PBC: polarization beam combiner, PBS: polarization beam splitter, PC: polarization controller.)

To further verify the performance of the proposed MFI, we conduct experiments for a 28 Gbaud hitless flexible coherent transceiver. The setup as well as Tx/Rx DSP are shown in Fig. 11(a)-11(c). For DSP at the Tx, the hitless rate change is realized by format switching. The 28 Gbaud electrical signals is generated by an arbitrary waveform generator (AWG, Keysight M9502A) and sent to I/Q modulator. At both Tx and Rx, 100-kHz external cavity lasers (ECLs) are used as the optical carrier and the LO, respectively. After being amplified by an Erbium-doped fiber amplifier (EDFA), the optical signal is launched into a re-circulating fiber loop consisting of 75-km SSMF and an EDFA. An optical spectrum analyzer (OSA, YOKOGAWA AQ6370C) is employed to monitor the OSNR. At the Rx, after the coherent detection, the signal is captured and digitized by 80 GSa/s digital sampling oscilloscope (Lecroy, Labmaster10-36Zi-A). The Rx DSP is shown in Fig. 11(c). After the CD compensation, downsampling, timing recovery, and CMA pre-equalization, the MFI is performed with FOC simultaneously. Please note that for 32QAM, we use method in [19] for FOC. The obtained information is used to adjust the following DSP modules, including decision directed-least mean square (DD-LMS) based equalization bundled with blind phase

Optics EXPRESS

search (BPS) based carrier phase recovery (CPR), and de-mapping/coding. The BER of B2B transmission is measured as a reference for performance evaluation, as shown in Fig. 11(d). The measured required OSNRs to reach BER=2×10^{-2} are 10.4 dB, 17.5 dB, 21.7 dB, and 28.8 dB for DP-QPSK/16QAM/32QAM/64QAM, respectively.

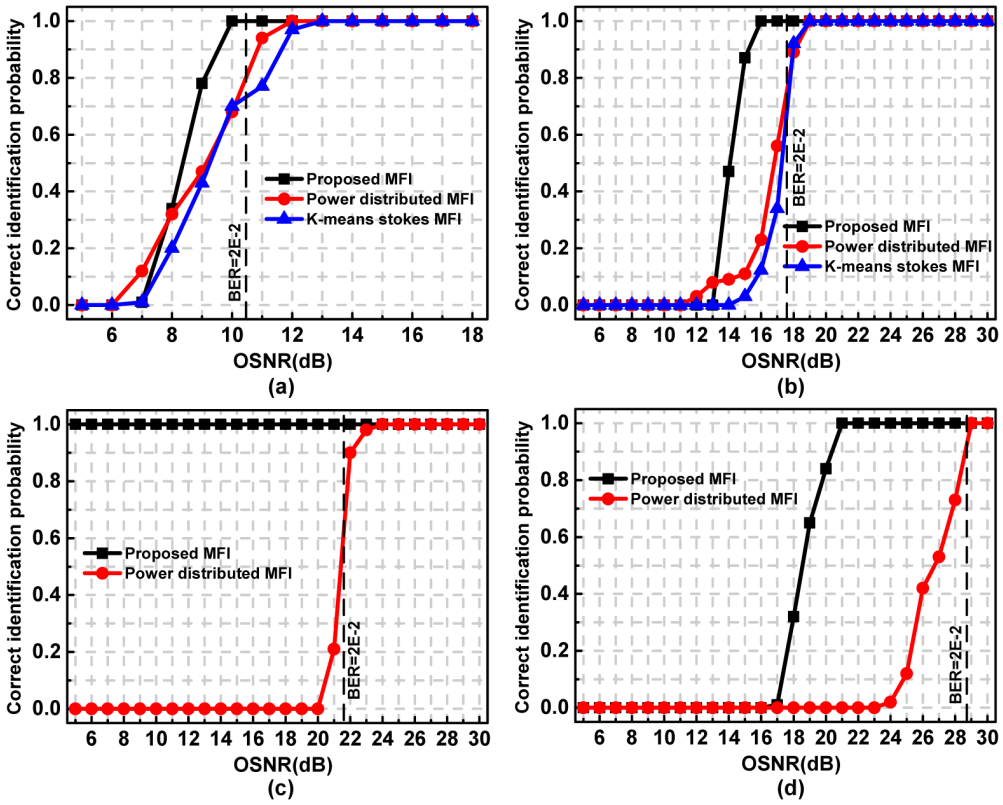

Fig. 12. Correct probability of MFIs versus OSNR under the scenario of B2B transmission. (a) DP-QPSK, (b) DP-16QAM, (c) DP-32QAM, and (d) DP-64QAM.

We evaluate the correct identification probability of the proposed MFI. For comparison, the performances of the k-means clustering based Stokes MFI [9] and the power distributed based MFI [13] are also provided. For the proposed MFI, 1024 symbols from both polarizations are used for one identification, while for k-means clustering based Stokes MFI, 4000 pairs of symbols are used. For the power distributed based MFI, it requires 10000 symbols [13]. Please note that for 32/64QAM, k-means clustering based Stokes MFI is not employed due to huge iteration times. For each case, 2000 times independent MFI are carried out to calculate the correct identification probability. As shown in Fig. 12, the accuracy of our proposed MFI is better than that of other two MFIs. Specifically, 100% MFI accuracy can be achieved even though the OSNR is lower than that required to reach BER=2×10^{-2} for each format using proposed MFI. The proposed MFI outperforms the power distributed based MFI especially for 32 and 64QAM. The performances of the power distributed based MFI degrade rapidly for high-order QAM, which is more easily to be disturbed by the noise. We also evaluate the performance of MFI after SSMF transmission, as shown in Fig. 13. The proposed MFI still remarkably outperforms other MFIs. For QPSK, three MFIs can all support over 1500 km SSMF. However, for other three formats, the accuracies of other two MFIs decrease dramatically, while the proposed MFI can still maintain 100% accuracy over 1500 km, 1500 km, and 825 km SSMF for 16QAM, 32QAM, and 64QAM.

Optics EXPRESS

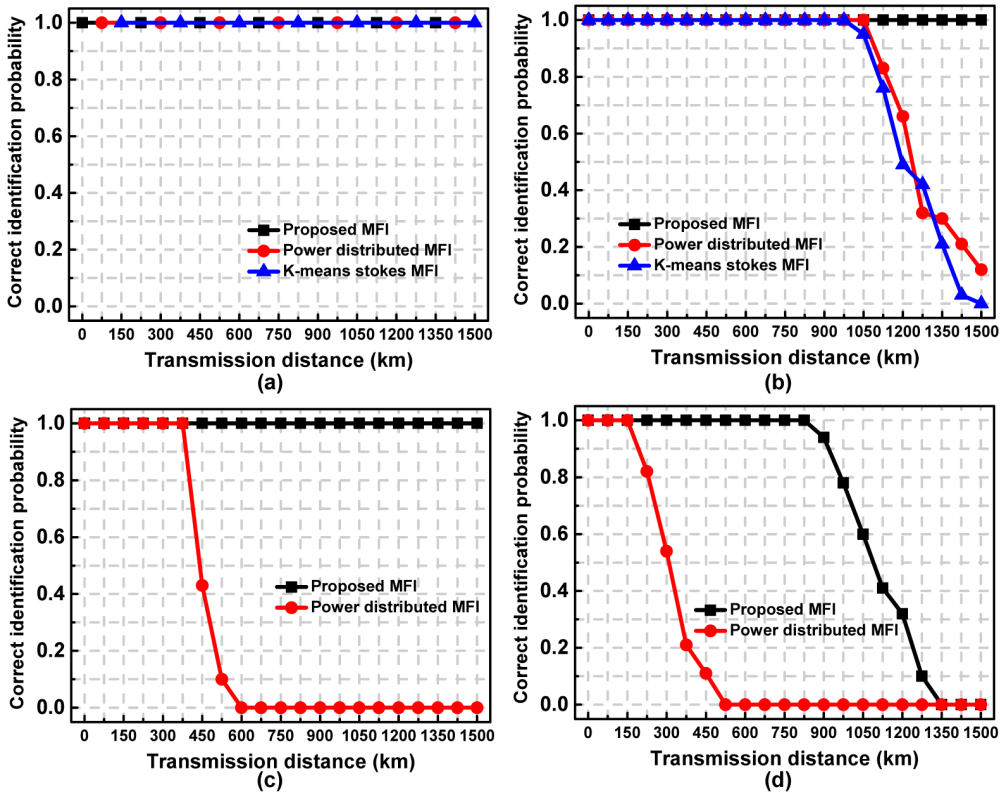

Fig. 13. Correct probability of MFIs versus SSMF transmission length. (a) DP-QPSK, (b) DP-16QAM, (c) DP-32QAM, and (d) DP-64QAM.

Finally, we demonstrate a hitless flexible coherent transceiver enabled by the proposed MFI with fast block-by-block format switching. Interleaved blocks are switched between DP-16QAM and DP-32QAM after the 900 km SSMF transmission or between DP-32QAM and DP-64QAM under the B2B scenario. Each block contains 2048 symbols (1024 symbols from both polarizations). As shown in Fig. 14, for the same format, the corresponding BERs and SNRs are stable, indicating hitless rate change can be realized by the proposed MFI. A little SNR fluctuation occurs mainly due to the limited number of symbols during the measurement.

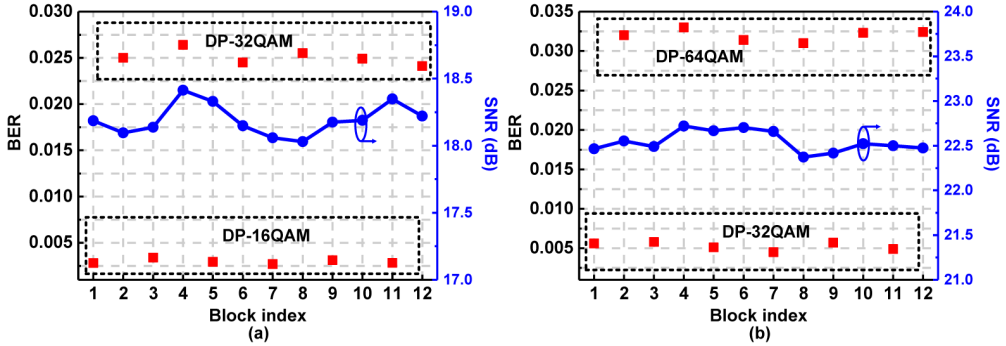

Fig. 14. BER and SNR versus block index for interleaved (a) DP-16QAM and DP-32QAM over 900 km SSMF transmission, (b) DP-32QAM and DP-64QAM under B2B transmission.

Optics EXPRESS

5. Complexity analysis

Table 1. Complexity comparison of proposed MFI

Step	Operation	Real multipliers	Real adders	Comparators
1	4th power transform	$4\times512\times8$	$4\times512\times2$	0
	FFT	$4\times512\times log_2512$	$4\times512\times log_2512$	0
	Adding up spectrums	0	512×3	0
	Peak selection	0	0	512-1
	PAPR calculation	2	512-1	0
	Comparing with threshold	0	0	1
	FO compensation	$4\times512\times4$	$4\times512\times2$	0
2	Partition scheme I	$2\times512\times4$	512×4	$6\times512\times4$
	Aliasing	0	$8\times(16-1)\times256/16$	0
	S-FFT	$8\times256/16\times log_2256/16$	$8\times256/16\times log_2256/16$	0
	Adding up spectrums	0	$256/16\times7$	0
	PAPR calculation	2	256/16-1	0
	Comparing with threshold	0	0	1
3	Partition scheme II	0	0	$2\times512\times4$
	Aliasing	0	$4\times(16-1)\times512/16$	0
	S-FFT	$4\times512/16\times log_2(512/16)$	$4\times512/16\times log_2(512/16)$	0
	Adding up spectrums	0	$512/16\times3$	0
	PAPR calculation	2	512/16-1	0
	Comparing with threshold	0	0	1
Total	/	48262	35965	16897

For practical realization of hitless flexible coherent transceiver, the hardware efficiency is of great importance. As analyzed in Section 2.1 and 2.2, the proposed MFI is based on the FFT-FOE. In point-to-point fixed optical network, the FFT-FOE is operated in a periodic manner due to the relatively slow FO drifting. However, for flexible network, the received signals can be transmitted from various locations with different FO. FFT-FOE should be operated for each signal block. Here, we provide complexity analysis of the proposed MFI in Table 1. Conventional FFT-FOE requires 43008 real multipliers and 28160 real adders in step 1. For S-FFT based step 2 and step 3, only 5254 additional real multipliers and 7805 additional real adders are required for implementation of two partition schemes, S-FFT, and PAPR calculation. The proportions of additional real multipliers and adders required for the MFI are only 12.22% and 27.72% of that for compulsory FFT-FOE. Due to the use of S-FFT, the complexity of step 2 and step 3 is reduced significantly. The extra hardware cost is mainly from comparators, whose complexity is much lower than multipliers and adders. Therefore, the proposed MFI is very hardware-efficient without much additional complexity.

6. Conclusions

A blind and efficient MFI scheme is proposed for hitless flexible coherent transceiver. Based on 4th power transform and partition of QPSK-like points, the proposed MFI shows high accuracy for QPSK and 16/32/64QAM. Moreover, the complexity is substantially reduced by

Optics EXPRESS

S-FFT. A hitless flexible coherent transceiver based on the proposed MFI is experimentally verified with fast format switching between 64QAM-32QAM and 32QAM-16QAM.

Funding

Hong Kong PhD Fellowship Scheme (HKPFS); National Natural Science Foundation of China (NCFC) (61435006); The Hong Kong Polytechnic University project (4-BCCK).

References

1. V. N. I. Cisco, Forecast, "Cisco visual networking index: forecast and methodology 2013-2018" (Cisco, 2016). http://www.cisco.com/c/en/us/solutions/collateral/service-provider/ip-ngn-ip-next-generation-network/white_paper_c11-481360.html.
2. I. Tomkos, S. Azodolmolky, J. Sole-Pareta, D. Careglio, and E. Palkopoulou, "A tutorial on the flexible optical networking paradigm: state of the art, trends, and research challenges," Proc. IEEE **102**(9), 1317–1337 (2014).
3. H. Khodakarami, B. Pillai, B. Sedighi, and W. Shieh, "Flexible optical networks: an energy efficiency perspective," J. Lightwave Technol. **32**(21), 3958 (2014).
4. A. Nag, M. Tornatore, and B. Mukherjee, "Optical network design with mixed line rates and multiple modulation formats," J. Lightwave Technol. **28**(4), 466–475 (2010).
5. V. N. Rozental and D. A. Mello, "Hitless rate switching for dynamically reconfigurable optical systems," IEEE Photonics J. **7**(2), 1–9 (2015).
6. K. Roberts and C. Laperle, "Flexible transceivers," in *European Conference on Optical Communication 2014 (ECOC)*, paper We.3.A.3.
7. M. Xiang, Q. Zhuge, M. Qiu, X. Zhou, F. Zhang, M. Tang, D. Liu, S. Fu, and D. V. Plant, "Modulation format identification aided hitless flexible coherent transceiver," Opt. Express **24**(14), 15642–15655 (2016).
8. M. Xiang, Q. Zhuge, M. Qiu, X. Zhou, M. Tang, D. Liu, S. Fu, and D. V. Plant, "RF-pilot aided modulation format identification for hitless coherent transceiver," Opt. Express **25**(1), 463–471 (2017).
9. R. Boada, R. Borkowski, and I. T. Monroy, "Clustering algorithms for Stokes space modulation format recognition," Opt. Express **23**(12), 15521–15531 (2015).
10. R. Borkowski, D. Zibar, A. Caballero, V. Arlunno, and I. T. Monroy, "Stokes space-based optical modulation format recognition for digital coherent receivers," IEEE Photonics Technol. Lett. **25**(21), 2129–2132 (2013).
11. T. Bo, J. Tang, and C. C. K. Chan, "Modulation format recognition for optical signals using connected component analysis," IEEE Photonics Technol. Lett. **29**(1), 11–14 (2017).
12. F. N. Khan, K. Zhong, W. H. Al-Arashi, C. Yu, C. Lu, and A. P. T. Lau, "Modulation format identification in coherent receivers using deep machine learning," IEEE Photonics Technol. Lett. **28**(17), 1886–1889 (2016).
13. J. Liu, K. Zhong, Z. Dong, C. Guo, A. P. T. Lau, Y. Lu, and Y. Lu, "Signal power distribution based modulation format identification for coherent optical receivers," Opt. Fiber Technol. **36**, 75–81 (2017).
14. G. Liu, R. Proietti, K. Zhang, H. Lu, and S. J. Ben Yoo, "Blind modulation format identification using nonlinear power transformation," Opt. Express **25**(25), 30895–30904 (2017).
15. J. Lu, S. Fu, L. Deng, M. Tang, Z. Hu, D. Liu, and C. C. K. Chan, "Blind and Fast Modulation Format Identification by Frequency-offset Loading for Hitless Flexible Transceiver," in *The Optical Fiber Communication Conference and Exhibition 2018 (OFC)*, paper M2F.5. pp. 1–3.
16. H. Hassanieh, P. Indyk, D. Katabi, and E. Price, "Simple and Practical Algorithm for Sparse Fourier Transform," ACM-SIAM Symposium on Discrete Algorithms (2012), p. 1183.
17. H. Hassanieh, F. Adib, D. Katabi, and P. Indyk, "Faster GPS via the Sparse Fourier Transform," in Proceedings of the 18th Annual International Conference on Mobile Networking and Computing (2012), **6**, p. 353.
18. J. Lu, X. Li, S. Fu, M. Luo, M. Xiang, H. Zhou, M. Tang, and D. Liu, "Joint carrier phase and frequency-offset estimation with parallel implementation for dual-polarization coherent receiver," Opt. Express **25**(5), 5217–5231 (2017).
19. F. Xiao, J. Lu, S. Fu, C. Xie, M. Tang, J. Tian, and D. Liu, "Feed-forward frequency offset estimation for 32-QAM optical coherent detection," Opt. Express **25**(8), 8828–8839 (2017).